Cell Stem Cell
Article

Dynamic Changes in Intracellular ROS Levels Regulate Airway Basal Stem Cell Homeostasis through Nrf2-Dependent Notch Signaling

Manash K. Paul,[1,8] Bharti Bisht,[1,8] Daphne O. Darmawan,[1] Richard Chiou,[1] Vi L. Ha,[1] William D. Wallace,[2] Andrew T. Chon,[1] Ahmed E. Hegab,[3] Tristan Grogan,[4] David A. Elashoff,[4,5] Jackelyn A. Alva-Ornelas,[1] and Brigitte N. Gomperts[1,5,6,7,*]
[1]Department of Pediatrics, Mattel Children's Hospital, University of California, Los Angeles, Los Angeles, CA 90095, USA
[2]Department of Pathology, University of California, Los Angeles, Los Angeles, CA 90095, USA
[3]Division of Pulmonary Medicine, Department of Medicine, Keio University Medical School, Tokyo 160-8582, Japan
[4]Department of Biostatistics, University of California, Los Angeles, Los Angeles, CA 90095, USA
[5]Pulmonary Medicine, University of California, Los Angeles, Los Angeles, CA 90095, USA
[6]Jonsson Comprehensive Cancer Center, University of California, Los Angeles, Los Angeles, CA 90095, USA
[7]Eli and Edythe Broad Stem Cell Research Center, University of California, Los Angeles, Los Angeles, CA 90095, USA
[8]Co-first author
*Correspondence: bgomperts@mednet.ucla.edu
http://dx.doi.org/10.1016/j.stem.2014.05.009

SUMMARY

Airways are exposed to myriad environmental and damaging agents such as reactive oxygen species (ROS), which also have physiological roles as signaling molecules that regulate stem cell function. However, the functional significance of both steady and dynamically changing ROS levels in different stem cell populations, as well as downstream mechanisms that integrate ROS sensing into decisions regarding stem cell homeostasis, are unclear. Here, we show in mouse and human airway basal stem cells (ABSCs) that intracellular flux from low to moderate ROS levels is required for stem cell self-renewal and proliferation. Changing ROS levels activate Nrf2, which activates the Notch pathway to stimulate ABSC self-renewal and an antioxidant program that scavenges intracellular ROS, returning overall ROS levels to a low state to maintain homeostatic balance. This redox-mediated regulation of lung stem cell function has significant implications for stem cell biology, repair of lung injuries, and diseases such as cancer.

INTRODUCTION

Reactive oxygen species (ROS) that were previously thought to be solely detrimental have more recently been found to have useful roles in stem cell (SC) proliferation and differentiation (Wang et al., 2013). However, the functional significance of the ROS status in different types of SCs, the downstream signaling events, and the role of ROS in SC self-renewal for repair and homeostasis has been controversial (Hochmuth et al., 2011; Jang and Sharkis, 2007; Le Belle et al., 2011). Some SCs with high ROS levels have been found to be more proliferative than other SCs with low ROS levels, but in other tissues the opposite has been found (Naka et al., 2008; Nakamura et al., 2012; Wang et al., 2013). Thus, it is not clear whether this is a tissue-specific effect or whether the dynamic rather than absolute ROS levels matter for SC self-renewal. The central theme of our investigation is the interrogation of the ROS status in SCs and the downstream signaling pathways that effect their self-renewal and proliferation.

The tracheobronchial epithelium serves as the first line of defense of the airway and is constantly exposed to environmental hazards and oxidative stress-mediated injury. Thus, a tightly controlled mechanism of repair by resident airway basal stem cells (ABSCs) is required to maintain airway health (Hegab et al., 2011, 2012b; Rock and Hogan, 2011; Rock et al., 2009, 2010). Defects in the repair process result in debilitating diseases like cystic fibrosis, asthma, chronic obstructive pulmonary disease (COPD), and lung cancer (Rock and Hogan, 2011; Rock et al., 2010). Histologically, the adult tracheobronchial airways of mice and humans closely resemble each other and ABSCs are the adult tissue SCs for epithelium of the large airways for both species (Borthwick et al., 2001; Ghosh et al., 2013; Hegab et al., 2011; Hong et al., 2004; Rock et al., 2009; Snyder et al., 2009). ABSCs provide a useful model SC system to study the effect of oxidative signaling on SC self-renewal and this is likely to be relevant to adult SC populations in other tissues.

Redox regulated signaling pathways in SCs are not well elucidated, but links have been made with the PI3K/Akt (Le Belle et al., 2011), Wnt (Myant et al., 2013), and p38 MAPK and JNK (Morimoto et al., 2013) pathways. Nuclear factor erythroid-2-related factor 2 (Nrf2) together with its negative regulator Kelch-like ECH-associated protein 1 (Keap1) is one important redox sensor and has been shown to regulate *Drosophila* gut SC regulation (Hochmuth et al., 2011). Activation of the Nrf2-antioxidant response element (ARE) signaling pathway enhances the antioxidant capacity of a cell (Lee et al., 2005; Nguyen et al., 2009). However, very little is known about the exact role of the Nrf2/Keap1 sensor system in mammalian SC self-renewal and the downstream pathways that they regulate.

One of the fundamental homeostatic mechanisms in the body is the prevention of excessive self-renewal, which can otherwise lead to diseases such as cancer. Here, we investigated the role of ROS levels and the ROS-mediated downstream signaling in self-renewal, proliferation, and homeostasis of ABSCs. We show, in both mouse and human ABSCs, that it is not the absolute high or low ROS level in a SC, but rather the dynamic intracellular ROS flux from a low (ROS^{lo}) to a relatively elevated level (moderate state [ROS^{mod}]) within a SC that is required for SC self-renewal after injury. Additionally, we found that Nrf2 directly regulates Notch for SC self-renewal and that the whole ROS-Nrf2-Notch pathway is key for cellular homeostasis.

RESULTS

Intracellular ROS Flux from Low to Moderate Levels Regulates ABSC Self-Renewal and Proliferation

To investigate the redox status of ABSCs, we first examined the in vivo ROS pattern of ABSCs in the uninjured mouse tracheal epithelium using the ROS-sensitive dye dihydroethidium (DHE) and found that ABSCs have widely disparate endogenous ROS levels (Figure 1A). To better understand the role of this differential ROS status on self-renewal, fluorescence-activated cell sorting (FACS) mouse ABSCs (mABSCs) and human ABSCs (hABSCs) (Hegab et al., 2011, 2012b; Rock et al., 2009) were segregated into ROS^{lo} (bottom 20%) and ROS high (ROS^{hi}) (top 20%) using the ROS-sensitive dye H_2DCFDA (2′,7′-dichlorodihydrofluorescein diacetate) (Chuikov et al., 2010; Le Belle et al., 2011; Raj et al., 2011) (Figure 1B) and subjected to the in vitro tracheosphere assay (Figure 1C). This assay quantifies the self-renewal (serial propagation of spheres) and proliferation (number of spheres and diameter of spheres) of ABSCs in vitro (He et al., 2009). The ROS^{lo} sorted mABSCs and hABSCs yielded a higher number and larger tracheospheres with an increased capacity for serial propagation (Figures 1C and 1D) and higher proliferation potential as demonstrated by EdU (5-ethynyl-2′-deoxyuridine) incorporation compared to the ROS^{hi} and $ROS^{unselected}$ sorted cells (Figures 1E and 1F and Figures S1A–S1D available online). Furthermore, sorting of ROS^{lo}-derived spheres (from Passage 0 [P0] ABSCs) demonstrated that the ROS^{lo} ABSCs had altered their ROS levels and gave rise to both ROS^{hi} and ROS^{lo} subpopulations (Figure S1C). ROS^{lo} ABSCs from P0 spheres again produced more and larger secondary tracheospheres (P1) after passaging as compared to the ROS^{hi} subpopulation and this was true for all subsequent passages (Figures 1D and S1D). A similar phenotype was obtained using other ROS-sensitive dyes, DHE, and Mitosox (Figures S1E and S1F). Thus, mABSCs that are sorted as ROS^{lo} increase their ROS in culture and have a higher proliferative capacity compared to ABSCs that are sorted as ROS^{hi} and similar findings were observed in human ROS^{lo} ABSCs (Figure S1G**)**. ABSCs exhibiting ROS^{mod} levels showed similar self-renewal and proliferation potential to that of ROS^{lo} ABSCs in the tracheosphere assay (data not shown), suggesting that dynamic levels of ROS may be relevant for self-renewal. ROS^{lo} mABSC populations have similar gene expression for known basal cell markers as that of their ROS^{hi} counterparts, but are enriched for p63 and Keratin 5 (K5) expression (Figure S1H).

To examine the role of cellular redox status on self-renewal, we treated ROS^{lo} ABSCs with exogenous ROS by giving in vitro nontoxic concentrations of hydrogen peroxide (H_2O_2). Addition of H_2O_2 showed a dose-response relationship with cellular proliferation at lower concentrations of H_2O_2, while higher concentrations of H_2O_2 inhibited ABSC proliferation (Figures 1E and 1F). This response to exogenous ROS shows that it is not the ROS^{lo} status of the cell, but rather the increase in ROS in the initially ROS^{lo} sorted ABSCs to moderate levels (“ROS flux”) bringing the oxidative status of a cell to a “sweet spot” that increases their self-renewal and proliferation potential. A similar response was observed with other oxidants like paraquat (Hochmuth et al., 2011; Myant et al., 2013) (Figure S1I). To further prove that ROS flux is required for proliferation we scavenged the endogenous ROS in ROS^{lo} ABSCs with an antioxidant N-acetyl cysteine (NAC) (Le Belle et al., 2011; Myant et al., 2013; Raj et al., 2011). Lowering the ROS levels in the ABSCs significantly decreased their proliferation but this phenotype could be partially restored by increasing their ROS levels with the addition of H_2O_2 to the cultures (Figures 1E and S1J). A similar phenotype was also observed with hABSCs (data not shown). To further understand how ROS plays a role in ABSC self-renewal and proliferation, we examined changes in the percentage of K5+ (ABSC) and K8+ (early progenitor cells [EP]) cells in tracheosphere cultures and submerged monolayer ABSC cultures by altering ROS levels in ABSCs with H_2O_2 and NAC treatment. We found that NAC reduces the formation of both K5+ and K8+ cells (Figures 1G and S1K). Addition of other antioxidants, like reduced L-glutathione, yielded similar results (Figure S1L). We further modulated ROS levels of ROS^{hi} ABSCs and found that NAC partially rescued ABSC proliferation, while H_2O_2 caused complete inhibition of proliferation (Figure 1H). Thus maximal SC proliferation occurs when ROS levels increase from ROS^{lo} to ROS^{mod} (sweet spot) and higher or lower levels of ROS reduce SC proliferation in both mABSCs and hABSCs in vitro. To assess the possible source of endogenous ROS in ABSCs, NOX/DUOX inhibitor, DPI, and Apocynin were used and both inhibitors resulted in dose-dependent inhibition of sphere formation (Figure S1M) suggesting that NOX/DUOX as well as mitochondrial ROS (Figures S1E and S1F) may be the sources of endogenous ROS that regulate ABSC proliferation.

Effect of ROS Modulation on Symmetric versus Asymmetric ABSC Division

In vivo under steady-state conditions ABSCs are mostly quiescent and self-renew at a low level. We therefore used a polidocanol-induced mouse tracheobronchial epithelial injury model to study the airway epithelial repair process during conditions of enhanced cell turnover for repair (Borthwick et al., 2001). In this model, adult mice are given an intratracheal (i.t.) injection of 2% polidocanol (Figure S2A) that leads to sloughing of the airway epithelium (Figures S2B–S2D). The few remaining ABSCs spread out to cover the partially denuded epithelium and then start self-renewing. ABSC self-renewal peaks at 48 hr postpolidocanol injury (hpi) in wild-type (WT) mice without showing any signs of differentiation, therefore this time point was selected for further experiments (Figures 2A and S2C). At this time point the EP cell population (K8+) is also seen localized suprabasally to the ABSCs (Figure S2D).

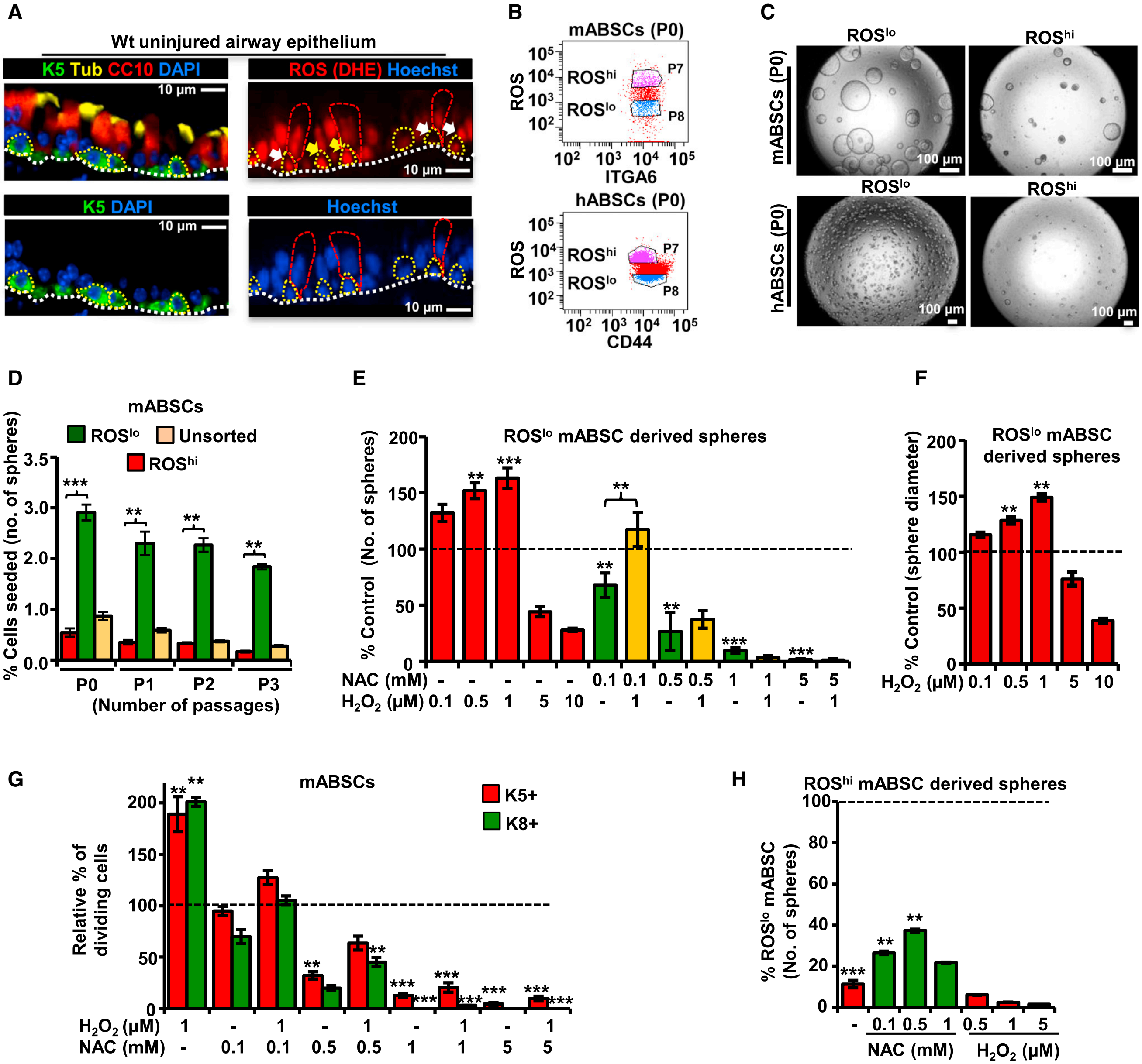

Figure 1. ROS Flux from Low to Moderate Levels Is Associated with Proliferation of ABSCs

(A) IF imaging of airway epithelium showing in vivo ROS. Left panel: the location of ABSCs (green), ciliated cells (yellow), and club cells (red). Dotted white lines show the basement membrane. Right panel: in vivo ROS staining of uninjured airway epithelium with DHE (hydroethidine), dotted yellow lines outline the ABSCs, and dotted red lines outline some differentiated cells. ROS^{hi} ABSCs (yellow arrows) and ROS^{lo} ABSCs (white arrows) are shown. Nuclei are stained with Hoechst dye (lower panels).

(B) Mouse ABSCs (mABSCs) and human ABSCs (hABSCs) were FACS-sorted on the basis of endogenous levels of ROS using H_2DCFDA and seeded in tracheosphere cultures.

(C) Bright field images of the primary tracheospheres (P0) at day 14 of culture.

(D) Primary mouse tracheospheres (P0) derived from ROS^{lo} mABSCs were dissociated after 14 days in culture and resorted into ROS^{lo} and ROS^{hi} populations and placed into the tracheosphere assay again. Serial passages were performed for three generations (P1–P3). Graph represents number of tracheospheres formed as a percentage of total number of mABSCs seeded.

(E) Effect of ROS modulation on tracheosphere formation of ROS^{lo} mABSCs. Bar graphs represent the number of tracheospheres formed as a percentage response to exogenous NAC and H_2O_2 treatment in comparison to control (dotted line).

(F) Bar graph representing diameter of mouse tracheospheres treated with H_2O_2.

(G) Bar graph representing relative percentage of dividing K5+ SCs and K8+ EP cells in sphere cultures treated with varying concentrations of H_2O_2 and NAC.

(H) Effect of ROS modulation on tracheosphere formation of ROS^{hi} mABSCs. Bar graphs represent the number of tracheospheres formed in response to exogenous NAC or H_2O_2 in comparison to control untreated ROS^{lo} mABSC (dotted line).

All data are presented as mean ± SEM. $^{*}p < 0.05$, $^{**}p < 0.01$, $^{***}p < 0.001$. See also Figure S1.

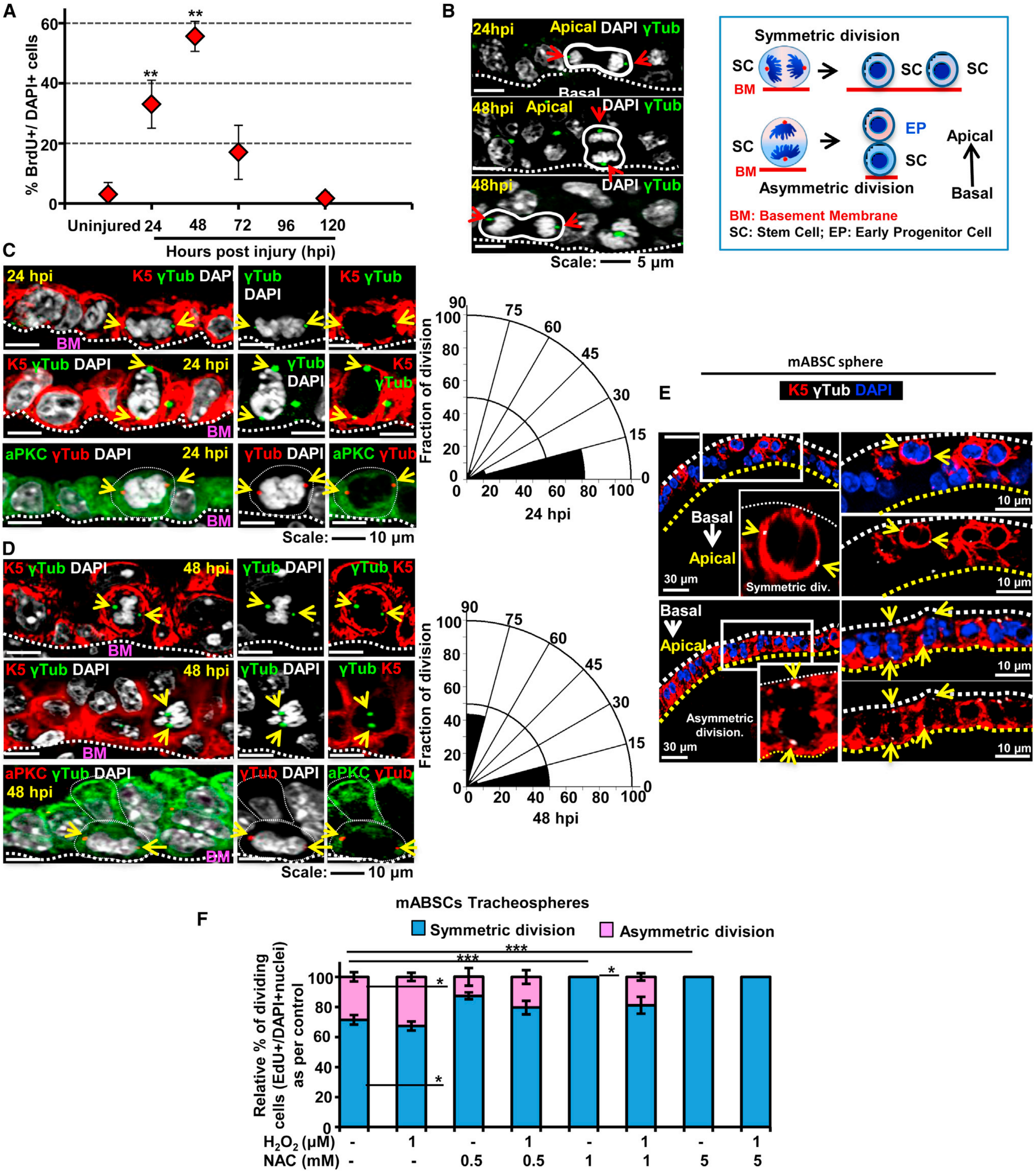
A
% BrdU+/ DAPI+ cells
0
20
40
60
**
**
Uninjured 24
48
72
96
120
Hours post injury (hpi)
B
24hpi
Apical DAPI γTub
Basal
48hpi Apical
DAPI γTub
48hpi
DAPI γTub
Scale: 5 μm
Symmetric division
SC
BM
SC
SC
SC
BM
EP
SC
Asymmetric division
Apical
Basal
BM: Basement Membrane
SC: Stem Cell; EP: Early Progenitor Cell
C
24 hpi
K5 γTub DAPI
γTub DAPI
K5 γTub
BM
aPKC γTub DAPI
γTub DAPI
aPKC γTub
Scale: 10 μm
Fraction of division
0
20
40
60
80
100
90
75
60
45
30
15
0
24 hpi
D
48 hpi
K5 γTub DAPI
γTub DAPI
γTub K5
BM
aPKC γTub DAPI
γTub DAPI
aPKC γTub
Scale: 10 μm
Fraction of division
48 hpi
E
mABSC sphere
K5 γTub DAPI
Basal
Apical
30 μm
Symmetric div.
10 μm
Basal
Apical
Asymmetric division.
30 μm
10 μm
F
mABSCs Tracheospheres
Symmetric division
Asymmetric division
Relative % of dividing cells (EdU+/DAPI+nuclei) as per control
0
20
40
60
80
100
***
***
*
*
*
H₂O₂ (μM) - 1 - 1 - 1 - 1
NAC (mM) - - 0.5 0.5 1 1 5 5

Figure 2. Characterization of the Polidocanol In Vivo Airway Epithelial Injury Model and Elucidation of Symmetrical versus Asymmetrical ABSC Division during Repair after Injury

(A) Graph representing the time course of in vivo epithelial proliferation for repair (% of BrdU+ve epithelial cells as compared to all DAPI+ nuclei) at different hpi. Data are presented as mean ± SEM (n = 10).

(B) DAPI staining of metaphase chromosomes and γ-tubulin immunostaining of centromeres in ABSCs (yellow arrows) demonstrates the plane of polarity for symmetrical versus asymmetrical division. Cartoon of symmetrical versus asymmetrical division. SC, stem cell; EP, early progenitor; BM, basement membrane.

(legend continued on next page)

To determine whether ABSCs are dividing symmetrically or asymmetrically, we examined a time course of in vivo airway epithelial repair after polidocanol injury and performed immunofluorescence (IF) staining for BrdU, K5, K8, γ-tubulin (to mark the angle of the mitotic spindle), and the polarity marker, atypical protein kinase C (aPKC). We examined the angle of spindle formation in comparison to the basement membrane (BM) in K5+ cells during the active repair process (Figures 2B–2D). We found that at 24 hpi when most of the epithelium is a single layer (Figure S2B) the K5+ basal cells divide symmetrically with horizontal angles of spindle formation (0° to 30° in relation to basement membrane) and equal distribution of aPKC immunostaining in both daughter ABSCs (Figure 2C) (Luxenburg et al., 2011). At 48 hpi the K5+ ABSCs show asymmetric division leading to a $K5^{hi}$ basal SC and $K5^{lo}$ EP cell (that subsequently loses K5 expression and becomes K8+ EP). These asymmetric divisions are characterized by apical distribution of aPKC (Figure 2D). No club or ciliated cells were observed at these early time points (24 and 48 hpi) (Figures S2C and S2D**)**.

We next assessed the effect of altering ROS levels on symmetric and asymmetric division in ABSC-derived tracheospheres during the ABSC proliferative phase at day 7 of culture (Figures 2E and 2F). We found that the relative percentage of symmetric versus asymmetric divisions did not change when ROS^{lo} ABSCS were treated with $H_2O_{2,}$ to reach the oxidative sweet spot for proliferation as compared to control untreated. However, NAC treatment, which results in a reduction in both K5+ ABSCs and K8+ EPs, did reduce the relative percentage of asymmetric divisions (Figure 2F).

In order to further examine self-renewal and proliferation of ABSCs (K5+) and EP cells (K8+) with modulation of ROS, we performed EdU staining of the H_2O_2 and NAC-treated and -untreated ABSCs in a submerged monolayer culture (Figure S2E) and quantified the numbers of K5+EdU+ ABSCs and K8+EdU+ EP cells (Gao et al., 2013). We found that varying ROS levels with H_2O_2 and NAC changes the proliferation of ABSCs and EPs relative to the control untreated, but the proportions of K5+ and K8+ cells in this assay remain similar (Figures S2F and S2G), **s**uggesting that probably both ABSC and EP proliferation is affected by modulation of ROS.

ROS Flux Regulates ABSC Proliferation In Vivo and In Vitro and Correlates with G1-M Transition During Cell Cycle

To understand the correlation of ROS flux with ABSC self-renewal, we examined ROS levels in tracheospheres as the ABSCs self-renew over time (Figure 3A). A significant increase in ABSC ROS levels was observed from days 3–7. These time points were chosen as during the initial phase of tracheosphere culture self-renewal is occurring in the absence of differentiation (data not shown). The rate of proliferation of ABSCs also increases from days 3–7 (Figure 3B). We found a significant positive correlation between the increase in ROS in the spheres and the proliferation of cells during sphere growth (Figures 3C), supporting the fact that the increase in ROS in ROS^{lo} ABSCs to ROS^{mod} levels supports ABSC proliferation.

We further examined in vivo ROS levels in live airway epithelium after polidocanol injury to determine the dynamic changes of ROS in the ABSCs in the repairing tracheal epithelium. We found an increase in ROS in the repairing ABSCs as compared to the uninjured controls and found a positive correlation between ROS status and proliferation in vivo (Figures 3D, 3E, and 2A).

To assess ROS flux at the single cell level during proliferation, we examined cell cycle dynamics of ABSCs together with their cellular ROS status (Sakaue-Sawano et al., 2008). To achieve this we visualized cell cycle progression in viable ABSCs using a FUCCI construct (Figure 3F) together with Cell ROX Red dye to correlate the phase of cell cycle and the level of ROS in each cell. We found a positive correlation between cell-cycle dynamics and cellular ROS status during the transition from G1 to G1-S which was maximal at G1-S phase ($p < 0.001$) (Figures 3G and 3H). Similar data was found in the actively dividing A549 lung cancer cell line (Figures S3A and S3B). Combining these results, we conclude that the ROS flux (low to moderate levels) in SCs serves as an intrinsic signal that sensitizes them for proliferation.

ROS Flux Mediates Nrf2-Induced ABSC Self-Renewal and Proliferation

Nrf2 and its repressor protein Keap1 are reported to act as major regulators of cellular redox levels (Sporn and Liby, 2012), and we therefore hypothesized that an increase in ROS flux can modulate Nrf2 activity. We analyzed expression of the Nrf2 downstream component NQO1 (NAD(P)H:Quinone Oxidoreductase I) (Suzuki et al., 2013) in proliferating spheres serially over time by western immunoblotting. An increase in NQO1 expression (but not Keap1) correlated with the increase in ROS production in spheres over time (Figure 4A), suggesting ROS-mediated Nrf2 signaling might be regulating ABSC proliferation.

We next modulated redox balance in vivo by using Nrf2 knock out (*Nrf2*$^{-/-}$) mice, (McDonald et al., 2010) which have higher ROS levels in ABSCs than wild-type (WT) controls (Figure 4B, upper panel). Similarly, hABSCs treated with Nrf2 siRNA exhibit higher ROS levels as compared to scrambled (SCR) siRNA controls (Figure 4B, lower panel). Loss of Nrf2 expression in both mice and humans (confirmed by western immunoblotting [WB]) (Figures S4A and S4B) leads to reduced proliferation of ABSCs in vitro with a lack of sphere formation, resembling that of the WT ROS^{hi} ABSC-derived sphere phenotype (Figures 4C and S4C–S4F) and showing again that a critical ROS level is needed for SC proliferation. No induction of early airway epithelial cell differentiation was seen in *Nrf2*$^{-/-}$ ABSC-derived spheres (Figures S4G and S4H). However, treatment with NAC

(C and D) The number of symmetrical versus asymmetrical cell divisions in the repairing airway epithelium at 24 hpi (C) and 48 hpi (D) was quantified with γ-tubulin and the polarity marker aPKC in radial histograms where symmetric divisions have spindle angles of 0° ± 30° while asymmetric divisions have spindle angles of 90° ± 30° in relation to the basement membrane.

(E) Symmetric and asymmetric division of mABSCs in tracheosphere cultures. γ-tubulin, white; K5, red.

(F) Quantification of the spindle angle of dividing mABSCs in sphere cultures in the presence of varying concentrations of NAC and H_2O_2.

All data are presented as mean ± SEM. $^{*}p < 0.05$, $^{**}p < 0.01$, $^{***}p < 0.001$. See also Figure S2.

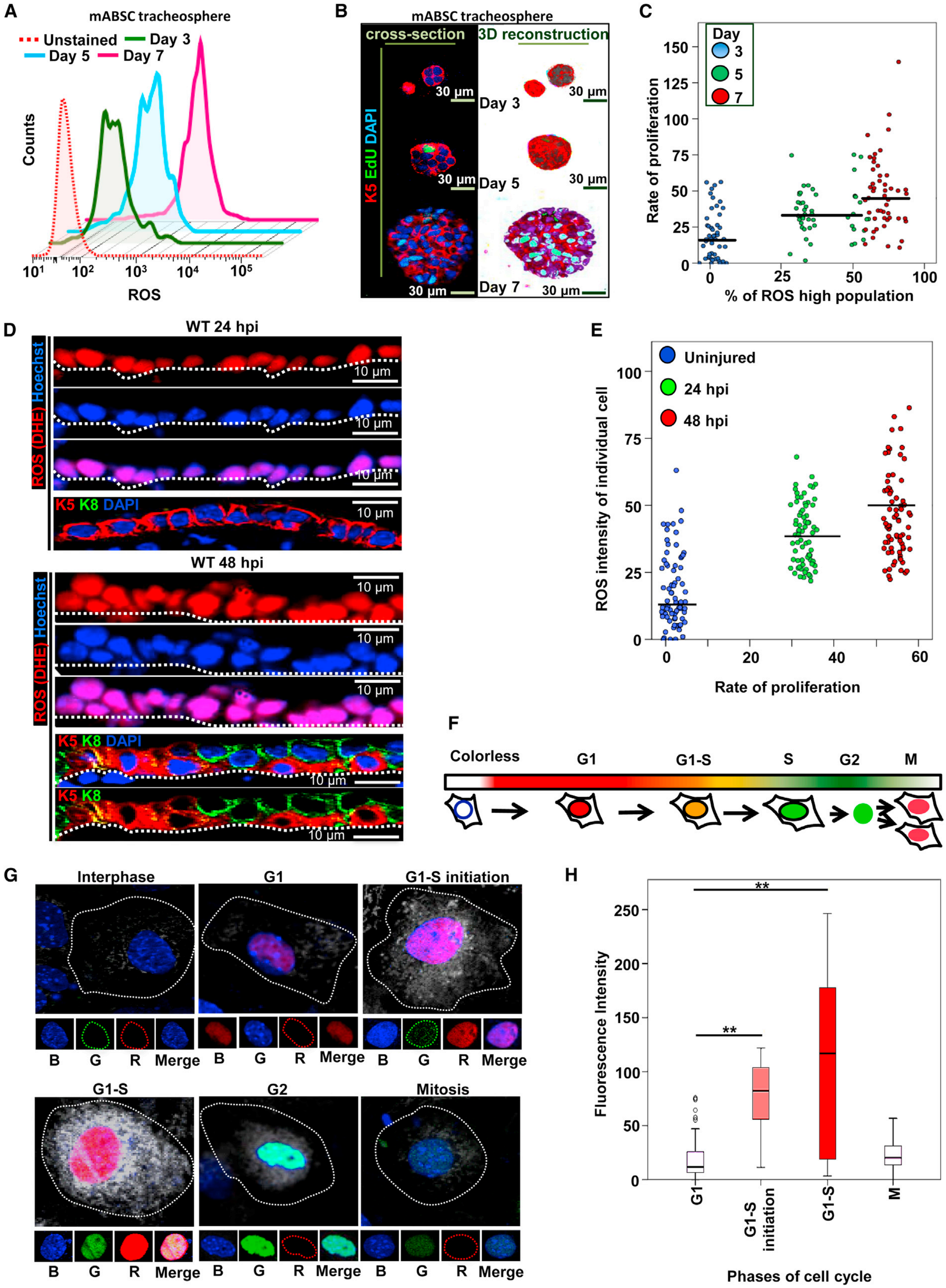

(legend on next page)

showed dose-dependent partial rescue of *Nrf2*$^{-/-}$ mABSC sphere formation (Figure 4D). Treating cells with a pan-caspase inhibitor (Z-VAD-FMK) demonstrated that apoptotic death of ABSCs was not the reason for the lack of sphere formation (Figure 4D). However, *Nrf2*$^{-/-}$ ABSCs were found to have increased senescence above WT ABSCs (Figures S4I and S4J). As our in vitro data indicated that the cellular redox sensor protein Nrf2 was activated during SC proliferation, we next examined Nrf2 downstream signaling events in vivo.

To examine the association between Nrf2 and self-renewal we performed immunohistochemistry (IHC) for Nrf2 and NQO1 in the tracheal epithelium under steady state conditions and after polidocanol treatment at 24 and 48 hpi. Nrf2 expression is rarely nuclear in the uninjured airway epithelium, while in WT repairing epithelium, Nrf2 exhibits nuclear localization in most cells at 24 and 48 hpi (Figure 4E). NQO1 expression is increased in repairing airway epithelium at 24 and 48 hpi (Figure 4E), further suggesting a role for Nrf2 in ABSC self-renewal for repair in vivo. As compared to WT, *Nrf2*$^{-/-}$ mice subjected to polidocanol injury showed delayed repair after injury at 48 hpi as seen by regular and transmission electron microscopy (Figures 4F and 4G) while the uninjured tracheas are morphologically similar to WT controls (Figure S4K). Moreover, the extent of injury of the airway epithelium was histologically similar in the WT and *Nrf2*$^{-/-}$ mice at 12 hpi (Figures 4F and 4H). *Nrf2*$^{-/-}$ mice showed a low level of self-renewal and proliferation after airway injury as indicated by BrdU incorporation, total cell counts, and K5+ and K8+ cell counts (Figures 4H–4K).

Notch Signaling Promotes ABSC Self-Renewal Downstream of Nrf2

To investigate Nrf2 downstream mediators, we screened different pathways with a candidate pathway luminescence array and found the Notch pathway to be significantly downregulated in the absence of Nrf2 in mABSC and hABSC (data not shown). We therefore examined the expression of Notch pathway components in Nrf2 knockdown (small interfering RNA [siRNA]) hABSCs by quantitative real-time PCR (qPCR) and found prominent downregulation of many Notch pathway components, suggesting a role for Nrf2 in regulating Notch ligand and receptor expression (Figure 5A). Similar data was obtained with *Nrf2*$^{-/-}$ mABSCs (data not shown). Notch1 has been reported to play a role in ABSC differentiation (Guseh et al., 2009; Rock et al., 2011), but the role of Notch in ABSC self-renewal was previously not studied. We first examined the presence of Notch pathway components in ABSCs as compared to differentiated airway epithelial cells by qPCR and found that ABSCs highly expressed Notch1, Delta1, Jagged1, and Jagged2 whereas Notch 2 and 3 were not differentially expressed (Figure S5A). To better understand the role of Notch pathway in self-renewal, WT mice were subjected to polidocanol treatment and the repairing airway epithelium was stained and analyzed by IF for activated Notch (NICD) and Notch pathway components at 24, 48, and 72 hpi. IF specificity of NICD antibody was confirmed by treating polidocanol airway-injured WT mice with the γ-secretase inhibitor, DBZ, and no nuclear NICD was detected (Figure S5B) (Guseh et al., 2009). The presence of NICD was observed in self-renewing ABSCs (BrdU+K5+) as well as proliferating EPs (BrdU+K8+) at different time intervals (Figures 5B and S5B–S5E). The Notch downstream basic Helix-Loop-Helix effector, Hes1, was expressed in many ABSCs, as well as EPs and differentiated cell types under steady-state conditions and during repair after injury (Figure 5C). Notch downstream bHLH effectors Hey1 and HeyL were upregulated during the repair process and were weakly expressed with almost no nuclear localization under steady-state conditions, suggesting they may play a key role in self-renewal (Figure 5C).

Notch1 activation was effected by transfecting ABSCs with a Notch1 constitutively active (ZEDN1, denoted as N^{act}) plasmid (Hicks et al., 2000) and culturing the ABSCs in a submerged monolayer culture (Gao et al., 2013). DBZ treatment of mABSC and hABSC monolayer cultures and tracheosphere cultures reduced ABSC proliferation, whereas activation of Notch resulted in mABSC and hABSC proliferation (Figures 5D, S5F, and S5G). Notch pathway activation and inactivation under these conditions was confirmed by WB (Figure S5H). ABSCs in the submerged monolayer cultures proliferate but do not differentiate at the time points studied (Figure S2F). The reduction in proliferation with DBZ treatment was confirmed in tracheospheres by quantifying sphere number and diameter (Figures 5E, 5F, S5I, and S5J) and by EdU staining (Figure S5K). In order to assess the effects of DBZ on K5+ and K8+ cell

Figure 3. ROS Flux from Low to Moderate Levels Is Associated with ABSC Proliferation and Cell Cycle Progression

(A) Representative FACS plot of ROS level, H_2DCFDA-stained tracheospheres from ROS^{lo} mABSCs at different days in culture (proliferation phase = 3, 5, and 7 days).

(B) Proliferation measured in spheres from different days in culture with EdU staining.

(C) Scattered correlation plot of the increase in ROS at different days of tracheosphere culture (% ROS high population) with the corresponding proliferation rate (EdU+/DAPI+ nuclei). The correlation was assessed using Spearman's rank correlation coefficient. A significant positive correlation was observed ($\rho = 0.505$, $p < 0.001$).

(D) IF imaging of airway epithelium showing in vivo ROS (DHE; red) at 24 and 48 hpi. Nuclei, Hoechst; K5, red; K8, green.

(E) Scattered correlation plot of the increase in ROS from uninjured to 24 and 48 hpi of the ABSCs in vivo (% ROS high population) with the corresponding proliferation rate (EdU+/DAPI+ nuclei) at same time points. The correlation was assessed using Spearman's rank correlation coefficient. A significant positive correlation was observed ($\rho = 0.571$, $p < 0.001$).

(F) Schematic representation of FUCCI transfected cells at different stages of cell cycle. mABSCs with cell cycle-specific FUCCI markers and ROS levels at different phases of cell cycle progression. G1 (nucleus red, marked by Cdt1-RFP), G1-S initiation (nucleus reddish orange, Cdt1-RFP and Geminin-GFP), G1-S (nucleus orange, Cdt-RFP and Geminin GFP), and M (nucleus green, Geminin GFP). R, red; G, green; ROS status (CellROX Deep Red dye), white dots; nuclei, Hoechst (B, blue).

(G) Three-dimensional merged representative images of mABSCs (n = 300) at different stages of cell cycle with their corresponding ROS status.

(H) Correlation between phase of cell cycle and ROS levels was assessed with a Kruskal-Wallis (KW) test. After the significant overall KW test ($p < 0.001$), follow-up Wilcoxon rank-sum tests were utilized to assess which phases were different. This post hoc analysis yielded statistically significant differences as shown.

See also Figure S3.

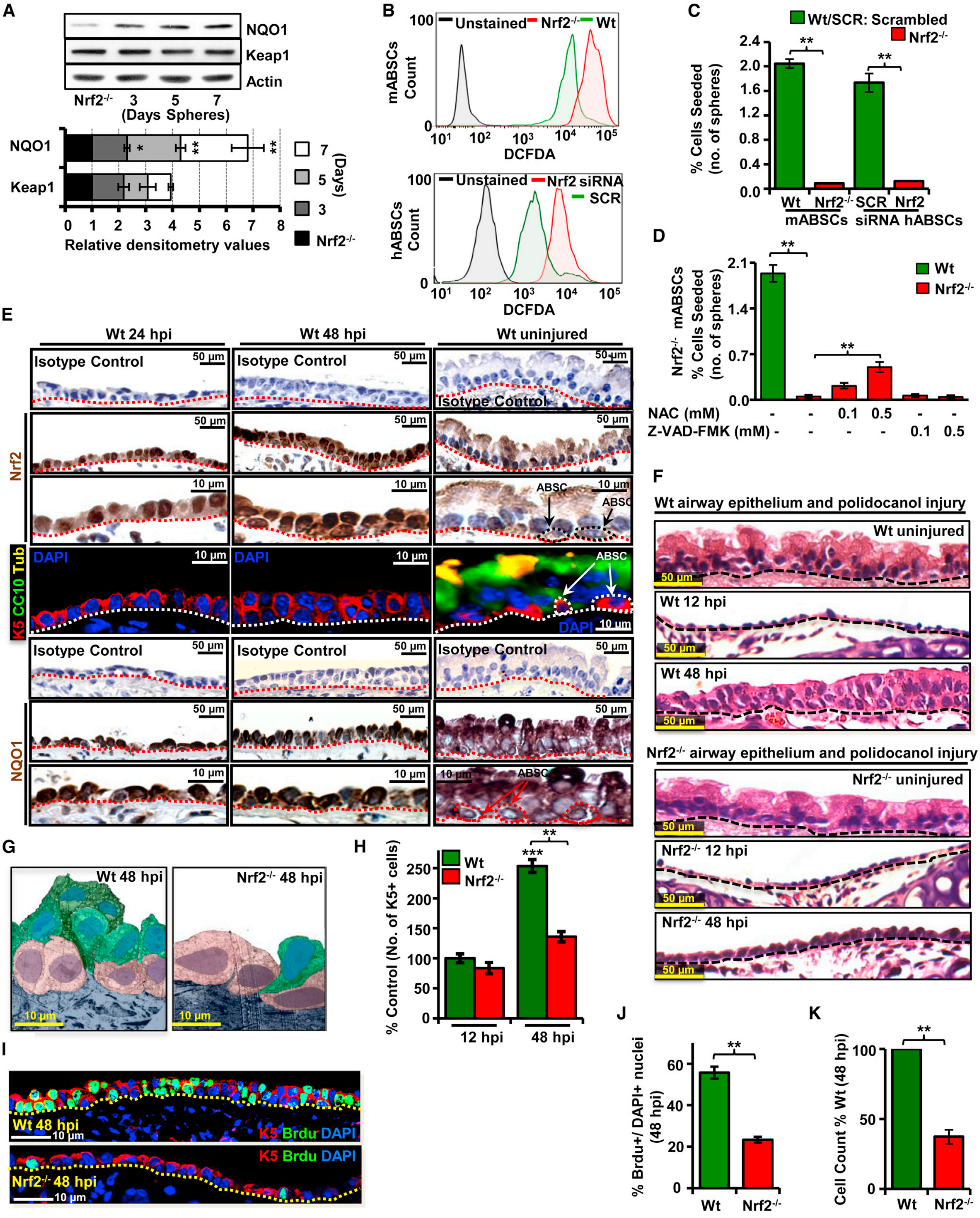

(legend on next page)

proliferation, we quantified the cell types in DBZ-treated spheres compared to control untreated spheres (Figures S5L and S5M). We found that DBZ inhibits both K5+ and K8+ cell proliferation in a dose-dependent manner. To demonstrate that the DBZ-induced reduction in ABSC self-renewal was not due to the early onset of ABSC differentiation, we examined the airway epithelial cell differentiation markers (serous polymeric immunoglobulin receptor [PIgR], mucus [MUC5Ac], club cells [CC10], and ciliated [acetylated β tubulin]), and no differences were seen compared to vehicle-treated controls (Figure S5M). Thus, the Notch pathway is important in self-renewal of ABSCs, and Notch modulation leads to alterations in proliferation in vitro.

Perturbation of Notch1 Signaling In Vivo Results in Alterations of ABSC Self-Renewal

To further dissect the role of Notch1 in ABSC self-renewal, we performed in vivo loss of function studies with intraperitoneal injections of DBZ in WT mice followed by a single i.t. DBZ injection at the same time as the i.t. polidocanol injury (Figure 6A). For Notch1 gain of function in vivo studies, we overexpressed the cytoplasmic domain of Notch1 (NICD) (Blanpain et al., 2006) specifically in ABSCs by crossing Rosa^{NICD} mice with K5-CrePR1 mice (Malkoski et al., 2010) (K5-CrePR1::Rosa^{NICD} [annotated K5-NICD]) (Figure 6A). K5-NICD and WT uninjured mice have a normal airway epithelium that has similar number and ratio of cell types, and RU486 does not alter the uninjured airway epithelium (Figures 6B, 6C, and S6A). The WT and K5-NICD mice airway epithelium showed similar extent of injury at 12 hr postintratracheal polidocanol administration (Figure S6A). The ABSC self-renewal was analyzed at 48 hpi, and we found significantly fewer K5+ cells in DBZ-treated airways as compared to vehicle-treated WT airways and K5-NICD airways after polidocanol injury ($p < 0.005$) (Figures 6B and S6B). Polidocanol injury in K5-NICD mice led to excessive self-renewal of ABSCs with a hyperplastic and dysplastic airway epithelium resembling premalignant lesions of the airway (Figures 6B–6D, S6B, and S6C). The self-renewal of ABSCs in these in vivo systems was further validated with total cell counts and EdU staining (Figures 6E and 6F). No differentiation was observed at 48 hpi under all experimental conditions (Figures 6B–6D). Together, these studies demonstrate that Notch1 signaling is involved in the self-renewal of ABSCs and the connection between ROS-Nrf2 and Notch signaling pathways may be important for repair.

Nrf2 Directly Regulates Notch1-Mediated ABSC Proliferation

In order to test whether Nrf2 regulates Notch1 for ABSC proliferation, we knocked down Nrf2 expression in both hABSCs and mABSCs and examined the expression of Notch1, Delta1, Jagged1, Hes1, and HeyL by WB and found them to be significantly downregulated (Figures S7A and S7B). We further examined Nrf2 regulation of Notch by qPCR for Notch pathway components in the repairing ABSCs after polidocanol injury in vivo in WT and *Nrf2*$^{-/-}$ mice. We found a significant increase in Notch pathway components in WT mABSCs at 48 hpi compared to WT uninjured mABSCs in vivo. However, loss of Nrf2 reduced mRNA expression of Notch1, Notch2, Notch3, Delta1, Jagged1, Jagged2, and Hey1 at 48 hpi (Figure 7A).

Sulforaphane is a chemical activator of Nrf2, and we found that it increases Nrf2 expression in ABSCs (Figure S7C) (Thimmulappa et al., 2002; Wakabayashi et al., 2010) but had no effect on ABSC proliferation in untreated submerged monolayer cultures as they are most likely proliferating maximally (Figures S7D and S7E). However, sulforaphane rescued DBZ-induced inhibition of ABSCs in the monolayer cultures (Figures S7D and S7E) and in the sphere assay (Figure S7F). To further confirm the relationship between Nrf2 and Notch1, we used a dual Notch reporter luciferase assay, CBF1-Luciferase reporter (Hicks et al., 2000) and found that sulforaphane treatment resulted in increased Notch reporter activity and could rescue DBZ-induced inhibition (Figure 7B). Thus, sulforaphane, acting as an Nrf2 activator, is also hyperactivating Notch and making DBZ less effective. We also used a genetic approach for studying Nrf2 activation in ABSCs by using Keap1$^{fl/fl}$ mice (Okawa et al., 2006). Keap1 ABSCs were FACS-sorted and transduced with adenoviral Cre-GFP (Ad-Cre) to effect a homologous Cre recombination leading to Keap1 inhibition. Ad-Cre untransduced ABSCs among the transduced ABSCs in culture serves as an endogenous control and the Keap1 knockout cells were characterized by WB (Figures S7G and S7H). We found that Ad-Cre transduced ABSCs formed more spheres and larger spheres than WT ABSCs and that Keap1-deficient ABSCs

Figure 4. ROS Flux Mediates Nrf2-Induced ABSC Proliferation

(A) Representative WB for NQO1 and Keap1 expression from *Nrf2*$^{-/-}$ ABSCs and ABSCs from serial days in tracheosphere cultures (days 3, 5, and 7) Lower panel: relative densitometric values compared with the basal levels in *Nrf2*$^{-/-}$ cells.

(B) Upper panel: a representative FACS plot of H_2DCFDA stained *Nrf2*$^{-/-}$ mABSCs. Lower panel: a representative FACS plot of H_2DCFDA-stained hABSCs treated with Nrf2-specific siRNA and scrambled (SCR) siRNA.

(C) Graph represents number of spheres formed with sorted mABSCs from *Nrf2*$^{-/-}$ mice as compared to WT mice and human sorted ABSCs transfected with Nrf2 siRNA and SCR siRNA.

(D) Graph represents number of spheres formed with FACS sorted *Nrf2*$^{-/-}$ mABSCs treated with different doses of NAC and a PAN caspase inhibitor.

(E) Immunohistochemistry for Nrf2 and NQO1 expression in the uninjured airway epithelium and at 24 and 48 hpi with isotype controls. IF for differentiation markers (CC10 and acetylated β-tubulin) at 24 and 48 hpi.

(F) Upper panel: the histology of uninjured WT mouse airway epithelium and the histology at 12 and 48 hpi. Lower panel: the histology of uninjured *Nrf2*$^{-/-}$ mouse airway epithelium and the histology at 12 and 48 hpi.

(G) Pseudo-colored TEM images of repairing airway epithelium at 48 hpi in WT and *Nrf2*$^{-/-}$ mice. mABSCs, purple; EP, green.

(H) Quantification of number of K5+ mABSCs at 12 and 48 hpi in *Nrf2*$^{-/-}$ versus WT mice.

(I) IF of WT and *Nrf2*$^{-/-}$ mice at 48 hpi for BrdU and K5 to examine proliferating mABSCs.

(J) Quantification of mABSC proliferation in WT and *Nrf2*$^{-/-}$ mouse repairing airway epithelium at 48 hpi.

(K) Quantification of total cell numbers in WT and *Nrf2*$^{-/-}$ mouse repairing airway epithelium at 48 hpi.

Data shown as mean ± SEM (n = 10). *$p < 0.05$, **$p < 0.01$, ***$p < 0.001$. See also Figure S4.

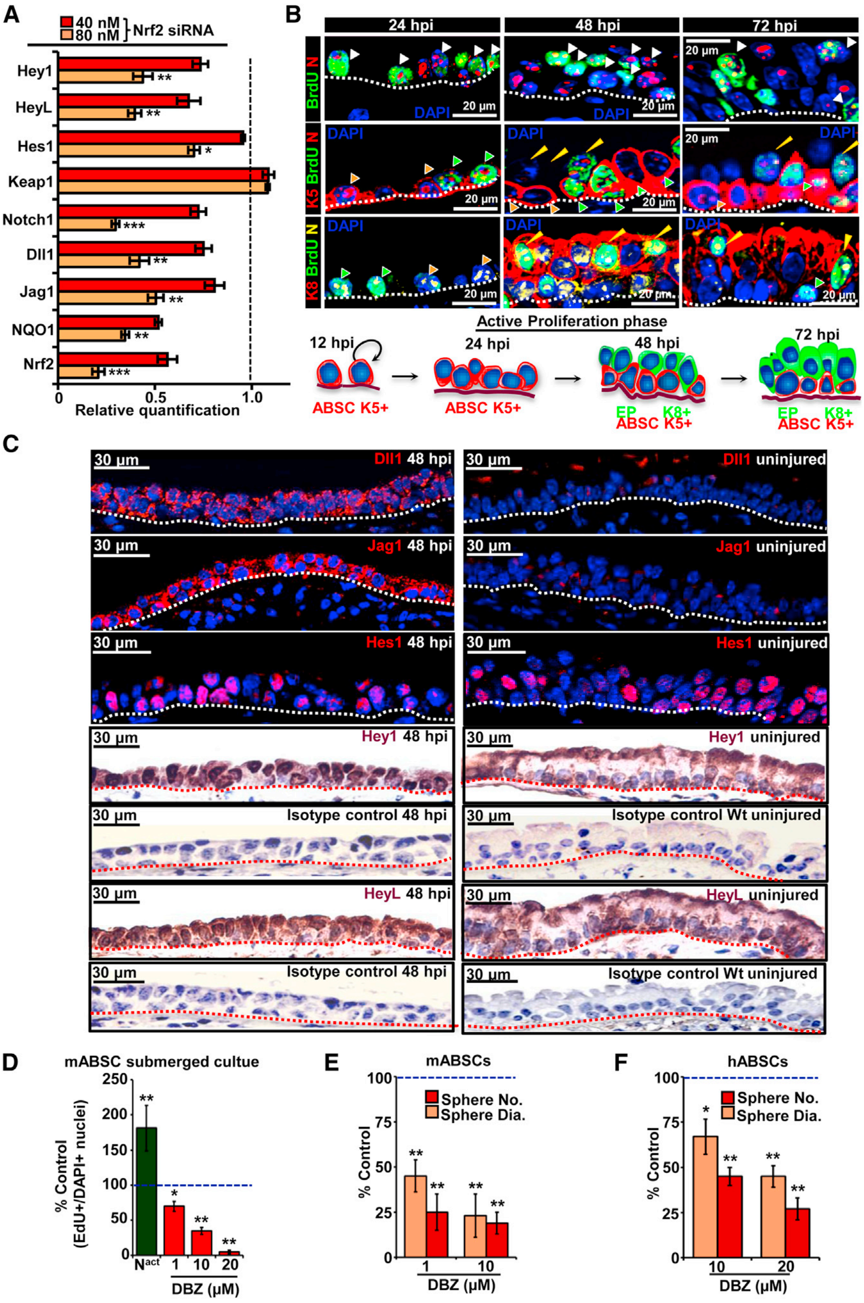

Figure 5. Notch Regulates ABSC Proliferation and Is Downstream of Nrf2

(A) qPCR analysis for Notch pathway components in hABSCs transfected with Nrf2 siRNA or SCR siRNA. Data are represented relative to SCR siRNA-transfected hABSCs, which is normalized to 1 (n = 3).

(B) Upper panel: Notch (N) immunostaining pattern (nuclear) in polidocanol-treated epithelium of WT tracheas at 24, 48, and 72 hpi. Middle panel: green arrowhead (K5+,Notch+,BrdU+ cells), orange arrowhead (K5+,Notch+,BrdU− cells), yellow arrowhead shows (K5−,Notch+,BrdU+ cells and likely represent EPs). Lower panel: green arrowhead (K8−,Notch+,BrdU+ cells and likely represent K5+ ABSCs), orange arrowhead (K8−,Notch+,BrdU− cells, likely represent nondividing K5+ cells), yellow arrowhead (K8+, Notch+, BrdU+ cells). The cartoon explains the repair process and the spatiotemporal localization of ABSCs and EPs.

(C) Sections of airway epithelium at 48 hpi as compared to uninjured airway immunostained with Notch pathway components; Dll1, Jag1, Hes1, Hey1, and HeyL, respectively, with isotype antibody controls.

(D) Notch levels were modulated in mABSCs monolayer cultures by treating cells with DBZ or Notch1 constitutively activating plasmid (N^{act}). ABSC proliferation was determined by calculating the ratio of EdU + cells divided by the total number of cells (DAPI+) compared with control.

(E and F) Mouse (E) and human (F) ABSC tracheosphere cultures were treated with DBZ and the sphere number and sphere diameter measured. Data are presented as mean ± SEM (n = 7). $^{*}p < 0.05$, $^{**}p < 0.01$, $^{***}p < 0.01$.

See also Figure S5.

could overcome the inhibition of DBZ treatment and rescue the sphere number and size to approximately WT levels (Figures 7C and S7I).

To further examine the role of Nrf2 in regulating Notch1 expression, we generated K5-Cre-PR1::$Rosa^{NICD}$::$\mathit{Nrf2}^{-/-}$ (annotated: KNN) triple transgenic mice. Ru486-uninduced ABSCs isolated from the KNN mice had approximately the same sphere size and sphere-forming ability as WT ABSC controls (data not shown). However, when Ru486 was used in vitro to induce K5-NICD in KNN ABSC-derived spheres, the spheres were approximately the size of WT spheres indicating that NICD was able to rescue the $\mathit{Nrf2}^{-/-}$ phenotype in the sphere assay (Figures 7D and S7J).

To further establish the Notch overexpression-mediated rescue of the $\mathit{Nrf2}^{-/-}$ phenotype in vivo, KNN mice were subjected to polidocanol injury. We found that the repair of KNN tracheal epithelium at 48 hpi was greater than WT and $\mathit{Nrf2}^{-/-}$ airway epithelial repair as determined by total cell counts and BrdU proliferation (Figures 7E, 7F, and S7K). Thus, the delayed repair seen in the $\mathit{Nrf2}^{-/-}$ airway after injury was rescued by activation of Notch, suggesting that Notch is downstream of Nrf2.

To further confirm Nrf2 regulation of Notch, we transfected ABSCs with Nrf2 plasmids harboring activating mutations (Nrf2 E82G and Nrf2 V36 del) (Ooi et al., 2013) and then examined Notch1 activity by qPCR. Notch1 expression was increased when Nrf2 was activated suggesting that Nrf2 is an upstream regulator of Notch in ABSCs (Figure 7G).

To demonstrate that there is a direct interaction of Nrf2 and Notch1 in ABSCs, we performed electrophoretic mobility shift assays (EMSAs) using nuclear extracts from mouse bronchoalveolar cells treated with sulforaphane. Incubation of nuclear extracts with the Notch1 ARE sequence resulted in a shift in its

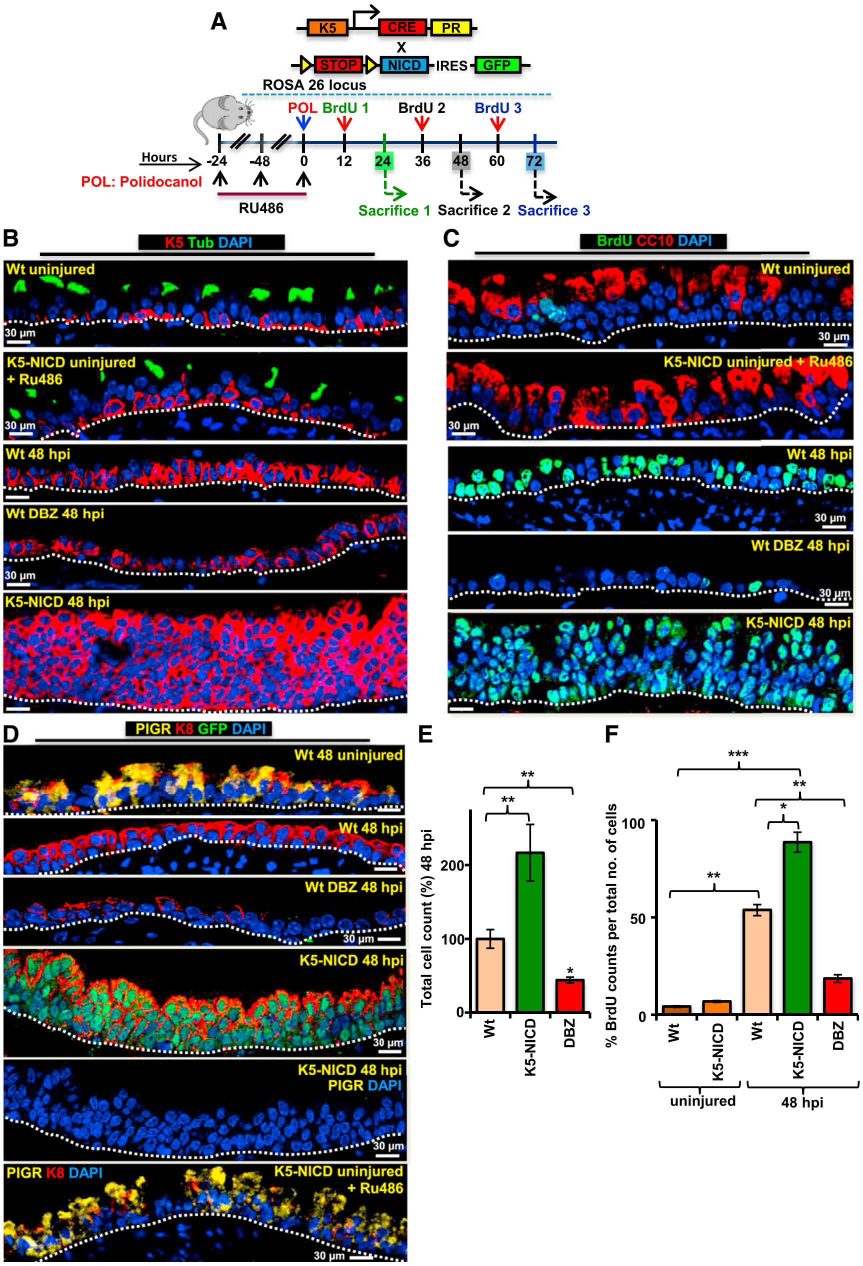
A
K5
CRE
PR
X
STOP
NICD
IRES
GFP
ROSA 26 locus
POL
BrdU 1
BrdU 2
BrdU 3
Hours
-24
-48
0
12
24
36
48
60
72
POL: Polidocanol
RU486
Sacrifice 1
Sacrifice 2
Sacrifice 3
B
K5 Tub DAPI
Wt uninjured
K5-NICD uninjured + Ru486
Wt 48 hpi
Wt DBZ 48 hpi
K5-NICD 48 hpi
30 μm
C
BrdU CC10 DAPI
Wt uninjured
K5-NICD uninjured + Ru486
Wt 48 hpi
Wt DBZ 48 hpi
K5-NICD 48 hpi
D
PIGR K8 GFP DAPI
Wt 48 uninjured
Wt 48 hpi
Wt DBZ 48 hpi
K5-NICD 48 hpi
K5-NICD 48 hpi PIGR DAPI
PIGR K8 DAPI
K5-NICD uninjured + Ru486
E
Total cell count (%) 48 hpi
0
100
200
Wt
K5-NICD
DBZ
**
**
*
F
% BrdU counts per total no. of cells
0
50
100
Wt
K5-NICD
Wt
K5-NICD
DBZ
uninjured
48 hpi
***
**
*
**

Figure 6. Notch Modulation Regulates ABSC Proliferation In Vivo

(A) K5-NICD breeding scheme and experimental plan.

(B–D) Representative IF images demonstrate differences in the repairing tracheas from the WT uninjured, K5-NICD uninjured and treated with RU486, WT (vehicle-treated) 48 hpi, WT DBZ-treated 48 hpi, and K5-NICD (with Ru486) 48 hpi. BrdU was examined for proliferation and acetylated β-tubulin, CC10, and PIgR were used as markers of differentiated cells.

(E and F) Bar graphs representing the total cell counts and proliferating cells seen under the in vivo experimental conditions. Data are presented as mean ± SEM (n = 7). $^*p < 0.05$, $^{**}p < 0.01$. See also Figure S6.

migration. Addition of Nrf2 antibody to the reaction resulted in a supershift of the complex, which was not seen with the IgG control. This demonstrates that Nrf2 binds directly to an ARE consensus site within the Notch1 promoter to regulate Notch1 transcription and therefore regulates canonical Notch signaling (Figure 7H) and points to a role for this interaction in regulating ABSC proliferation.

To further examine the interaction between Nrf2 and Notch in the regulation of proliferation, we examined cell-cycle-related genes in Nrf2 knockdown and Notch-activated conditions. We found that Nrf2 inhibition and Notch1 activation reciprocally alter the levels of pRB, Cyclin D1, and Cyclin B1, respectively, but not Rb (Figure S7L). This leads us to propose a model of a tightly regulated homeostatic process where the Nrf2 and Notch pathways act together to promote cell-cycle progression but are rapidly turned off when ROS levels drop (Figure 7I), thus maintaining cellular homeostasis.

DISCUSSION

Here, we identified a unifying model that explains ROS-induced SC self-renewal for repair after injury and that ROS-Nrf2-Notch pathway is a major effector of proliferation in the airway epithelium. We used mouse and human ABSCs to demonstrate that it is the dynamic intracellular ROS flux from low to moderate levels that regulates airway SC proliferation. During cell cycle progression there is also a flux of ROS at the G1-S transition and scavenging of ROS inhibits cell cycle, therefore it is likely that the change in ROS levels is linked to the cell cycle. In addition, our data suggest that ROS flux to moderate levels promotes both symmetric and asymmetric division of ABSCs, but ROS levels that are too low or too high have, as expected, reduced symmetric division but interestingly also highly reduced asymmetric division.

Nrf2 as the major effector of ROS in the cell regulates a number of ARE containing genes, including Notch1, to regulate proliferation and reduce ROS levels in the cell. Thus the ROS within the cell acts as a rheostat to regulate the Nrf2-Notch1 pathway, and the quiescent cell initially responds to an increase in ROS thereby allowing self-renewal for repair but when the ROS levels drop due to antioxidant production this inhibits proliferation in the same cell thereby preventing excessive proliferation that could be detrimental to the repairing tissue (Figure 7I).

This simple mechanism of flux of ROS explains the discrepancies in the current field regarding the levels of ROS found in

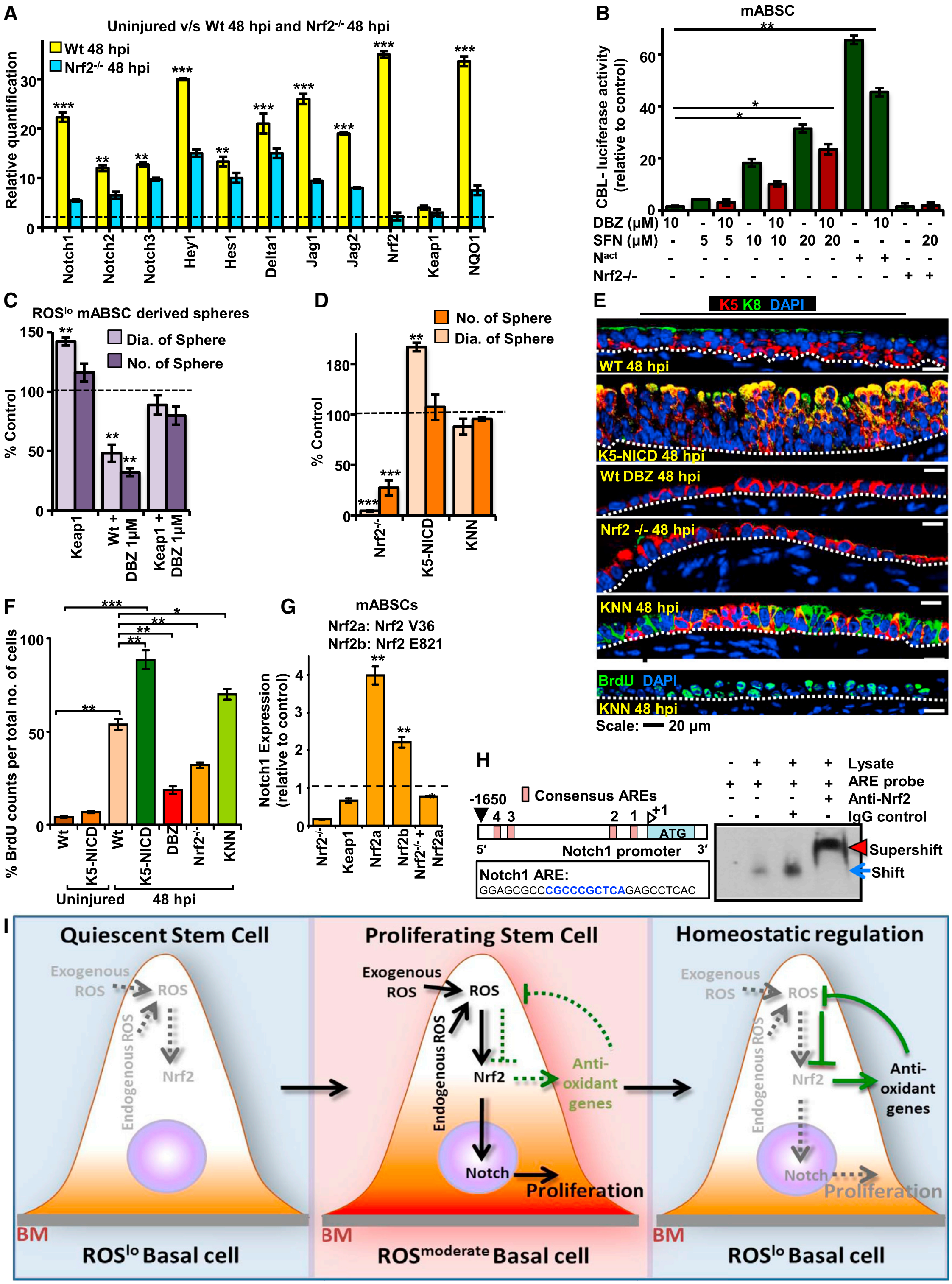

Figure 7. Nrf2 Directly Regulates Notch, which Activates ABSC Proliferation

(A) qPCR from FACS sorted mABSCs of the repairing airway epithelium of WT and *Nrf2*$^{-/-}$ mice at 48 hpi for Notch pathway components compared to uninjured airway epithelium (dashed line) (n = 13).

(B) Dual luciferase assay to study the interaction between Nrf2 and Notch by CBL-Luc Notch reporter luciferase activity in ABSCs in the presence of DBZ, the Nrf2 activator SFN, and a constitutively active Notch plasmid (N^{act}) (n = 6).

(C) Adenoviral-Cre-GFP was transduced into FACS-sorted Keap1$^{fl/fl}$ ABSCs. Keap1-deficient ABSCs were treated with DBZ and the number and size of the spheres was quantified. Dotted line represents WT untreated control.

(legend continued on next page)

other proliferating adult SCs and the role of ROS in SC self-renewal and proliferation. For example, mammalian quiescent hematopoietic SCs (HSCs) contain low levels of ROS and are considered to be proliferation proficient, while impairment of self-renewal and exhaustion of HSCs was observed with ROS^{hi} HSCs (Jang and Sharkis, 2007; Naka et al., 2008; Nakamura et al., 2012; Wang et al., 2013). Our results explain how ROS^{hi} sorted HSCs may not be able to self-renew in the short or long term as they would not be able to flux their ROS to moderate levels unless their antioxidant levels were increased to achieve this balance. In contrast to these studies, *Drosophila* gut SCs are reported to be ROS high (Hochmuth et al., 2011) and that ROS facilitates Wnt-driven intestinal SC proliferation leading to colorectal cancer (Myant et al., 2013). Our mechanism of ROS flux explains the higher levels of ROS in these gut SCs as they proliferate relatively rapidly and likely spend a greater amount of time with moderate levels of ROS. It is also important to consider that the balance of oxidants and antioxidants within a cell may be different for different cell types, and some cells may be more efficient at scavenging ROS than others and may flux ROS differently. This may explain why mammalian proliferative neuronal SCs in culture are relatively ROS high (Le Belle et al., 2011). In addition, published results from different groups are not standardized, so it is important to recognize that ROS levels that are reported as high from one group may represent moderate levels with respect to the findings from another group.

This report shows ROS-mediated activation of the Notch1 pathway in SCs and that Notch1 plays a vital role in ABSC self-renewal and proliferation. Previous studies have found Notch signaling to play a role in cell fate determination of the airway epithelium (Guseh et al., 2009; Rock et al., 2011; Tsao et al., 2009), but no information exists regarding the role of Notch in ABSC proliferation. Moreover, Rock et al. (2011) also showed that addition of DBZ causes inhibition of ABSC proliferation, which is similar to what we observed. Our study using NICD transgenic mice and pharmacologic inhibitors of Notch1 shows that Notch1 is indeed an important player in ABSC proliferation both in vitro and in vivo.

We speculate that the ROS-Nrf2-Notch pathway is a conserved pathway that is designed to allow cells to respond to changes in environmental levels of ROS. Our findings contain, to our knowledge, the first observation of ROS activation of Nrf2-Notch signaling in mouse and human SC self-renewal and proliferation. Our study is supported by the previous report of Nrf2-Notch interaction in total liver cells (Wakabayashi et al., 2010) and recently in HSC protection from radiation (Kim et al., 2014).

The airway epithelium is constantly exposed to environmental oxidants and therefore serves as an interesting model system to study redox signaling. Cigarette smoke is known to cause oxidative stress-induced airway injury, and airway diseases such as COPD and lung cancer are directly linked to smoking (Barreiro et al., 2010; Herbst et al., 2008). Our study emphasizes that loss of the normal ROS-Nrf2-Notch cellular homeostatic mechanism that prevents excessive proliferation might be associated with airway diseases and cancer. Chronic oxidative stress might lead to chronic activation of Nrf2 and this increased proliferative potential may lead to cancer. Recent data suggest that Nrf2 is activated in lung cancer and provides a protumorigenic advantage (Kansanen et al., 2013; Cancer Genome Atlas Research Network, 2012). On the contrary, a previous study in Nrf2 knockout mice showed that the absence of Nrf2 led to accelerated colonization and proliferation of lung cancer cells (Satoh et al., 2010). Interestingly it is reported that oncogene-induced Nrf2 transcription promotes ROS neutralization and pancreatic tumorigenesis (DeNicola et al., 2011). Oxidative stress also prevents Keap1 inhibition and results in Nrf2 activation. Our study suggests that activating mutations of Nrf2 and/or mutations leading to inhibition of Keap1 results in overactivation of downstream pathways, such as Notch, which drives hyperplasia in the airway epithelium. Notch activation is also reported in lung cancer (Westhoff et al., 2009), although the presence of inactivating mutations is also predicted (Cancer Genome Atlas Research Network, 2012) and Nrf2 and Notch are reported to be altered in COPD (Malhotra et al., 2008; Tilley et al., 2009).

Taken together, our data demonstrate a vital homeostatic mechanism that prevents the excessive proliferation of ABSCs but at the same time allows them to respond to injury and proliferate for repair. Identifying alterations in this pathway will likely lead to novel therapeutic strategies for hyperproliferative diseases.

EXPERIMENTAL PROCEDURES

Supplemental Experimental Procedures and any associated references can be found in the Supplemental Information.

(D) FACS-sorted mABSCs isolated from the WT, *Nrf2*$^{-/-}$, K5-NICD, and KNN mice were cultured in the sphere assay. The diameter and number of spheres were quantified from the brightfield images (Figure S7J). The dotted line represents WT control. Data are presented as mean ± SEM (n = 3).

(E) IF for K5, K8, and BrdU of the repairing airway epithelium at 48 hpi in WT, *Nrf2*$^{-/-}$, K5-NICD, DBZ-treated WT, and KNN mice.

(F) Quantification of BrdU in the repairing airway epithelium in uninjured WT, K5-NICD mice; *Nrf2*$^{-/-}$, K5-NICD, DBZ-treated WT, and KNN mice at 48 hpi. Data are presented as mean ± SEM (n = 8).

Significance was calculated by two-tailed, paired Student's t test. Values are as mean ± SEM. $^{*}p < 0.05$, $^{**}p < 0.01$, $^{***}p < 0.001$.

(G) mABSCs were transfected with two different known activating mutations of Nrf2 (Nrf2 V36 del [Nrf2a] and Nrf2 E821 [Nrf2b]). Notch expression was measured using qPCR. Notch expression was measured relative to WT untransfected ABSC control expression. Data are presented as mean ± SEM (n = 3).

(H) Cartoon showing the mouse Notch1 promoter and the ARE consensus sequences. The Notch ARE sequence used in the EMSA corresponds to ARE1, which is located between −204 and −196 bps upstream of the transcriptional start site. The Notch1 sequence used to generate probes for the EMSA is shown. The blue arrow shows the specific protein complex with the Notch1 probe, and the red arrowhead shows the super-shifted band after adding the Nrf2 antibody.

(I) Schematic model of ROS flux tightly regulating ABSC self-renewal and repair after injury. ABSCs demonstrate heterogeneity with regard to ROS status. ROS^{hi} ABSCs are proliferation-deficient and not shown. Quiescent ABSCs have a low level of ROS and after injury the ROS^{lo} ABSCs undergo a flux change in their ROS levels to ROS^{mod}. This flux activates Nrf2, which directly increases Notch1 expression and promotes self-renewal and proliferation for repair. Nrf2 also induces antioxidants that reduce ROS levels and this brings the ABSC back to the quiescent state with inhibition of proliferation in a tightly regulated fashion.
See also Figure S7.

ROS Measurements

ROS production was measured with ROS-sensitive dyes (H_2DCFDA, DHE, Mito Sox, and Cell ROX Deep Red) where cells were labeled with 5 μM of the H_2DCFDA dye as described previously (Chuikov et al., 2010; Le Belle et al., 2011; Raj et al., 2011). Please see Supplemental Experimental Procedures.

Induction of Epithelial Injury by Intratracheal Instillation of Polidocanol

Induction of airway epithelial injury was mediated by i.t. instillation of polidocanol (Sigma) (Borthwick et al., 2001). Briefly 6- to 8-week-old mice were anesthetized with isoflurane vaporized in a 3:1 mixture of O_2 and air and placed supine while anesthesia was maintained for the rest of the experiment. Airway injury was induced after anesthesia by i.t. administration of 10 μl of 2% polidocanol in PBS using a BD Insulin Syringe M/Fine 0.3 ml (31G). To assess the time course of injury and repair, mice were euthanized at 12, 24, 48, 72, and 120 hr after instillation of polidocanol and their tracheas were removed for histology.

Proliferation Assay and Immunofluorescence

The EdU incorporation assay was performed as per the company protocol using the Click-iT EdU kit (Invitrogen). In vivo proliferation was studied by BrdU incorporation in WT uninjured mice and after epithelial damage was induced by i.t. instillation of 2% polidocanol (Borthwick et al., 2001). For further details please see the Supplemental Experimental Procedures. IF was performed as described (Hegab et al., 2011, 2012a, 2012b; Rock et al., 2009, 2011) (Table S3).

Quantification of Spindle Orientation

Spindle orientation was quantified by comparing γ tubulin localization (centrosomal) in late metaphase and anaphase as compared to the axis of the basement membrane (BM) (Luxenburg et al., 2011). Please see Supplemental Experimental Procedures.

Nuclear Protein Extraction and EMSA

The sequences used to generate probes containing the Notch1 ARE were previously published (Wakabayashi et al., 2010). Probes were biotinylated using a Biotin 3′ End labeling Kit (Thermo Scientific) according to the manufacturer's instructions. EMSAs were performed and detected using the Chemiluminescent Nucleic Acid Detection Module (Thermo Scientific). Please see Supplemental Experimental Procedures.

Reporter Gene Assays

ABSCs were seeded in 48-well plates and transiently transfected with 1 μg of the Notch-dependent CSL luciferase reporter vector (Hicks et al., 2000), 0.8 μg expression plasmid, and 0.8 μg Renilla Luciferase reporter vector pRL-TK for standardization (Promega). Transfections were performed using Lipofectamine 2000 (Invitrogen). Cells were harvested after 48 hr and assayed for luciferase activity using the Dual-Luciferase Reporter Assay System (Promega), using a Turner Biosystems Luminescence plate reader.

For pathway screening, we used the Cignal finder reporter array, Development 10 pathway format (SA Biosciences-QIAGEN Company) as per manufacturer's instructions.

Statistical Analysis

Quantified data are expressed as the mean ± SEM values. Significance testing was conducted via Student's t test. Proliferation and its correlation with ROS production was assessed using Spearman's rank correlation coefficient. To investigate a possible correlation between ROS status with the cell cycle a Kruskal-Wallis (KW) test was run followed by Wilcoxon rank-sum test.

SUPPLEMENTAL INFORMATION

Supplemental Information includes Supplemental Experimental Procedures, seven figures, and four tables and can be found with this article online at http://dx.doi.org/10.1016/j.stem.2014.05.009.

AUTHOR CONTRIBUTIONS

M.K.P. and B.B. designed and conducted the experiments, data analysis, statistical analysis of the data and wrote the manuscript. D.D., R.C., V.H., and J.A.A. conducted the experiments. A.T.C. and A.E.H. provided technical support. T.G. and D.A.E. provided statistical analysis of the data. W.D.W. provided data analysis. B.N.G. designed the experiments, analyzed the data, and wrote the manuscript.

ACKNOWLEDGMENTS

We would like to thank Dr. William H. McBride for the *Nrf2*$^{-/-}$ mice and Dr. Kupiec-Weglinski and Dr. Yamamoto for the Keap1$^{fl/fl}$ mice. We thank Dr. Gerry Weinmaster for helpful discussions and reagents. pIRES Puro-Nrf2 V36 del and pIRES Puro-Nrf2 E821 mutant plasmids are kindly provided by Dr. Aikseng Ooi. We are grateful to Dr. K. Plath, Dr. V. Hartenstein, Dr. T. Chatila, Dr. D. Shackelford, and Dr. G. Crooks for critically reading the manuscript. This work was supported by California Institute for Regenerative Medicine (CIRM) (RN2-00904-1), National Heart, Lung, and Blood Institute (NHLBI) (HL094561), American Thoracic Society (ATS-06-065), the Concern Foundation, the UCLA Jonsson Comprehensive Cancer Center Impact Award, the UCLA Jonsson Comprehensive Cancer Center Thoracic Oncology Program/ Lung Cancer SPORE, the University of California Cancer Research Coordinating Committee, and the Gwynne Hazen Cherry Memorial Laboratories (to B.N.G.). We appreciate assistance from the UCLA Eli and Edythe Broad Stem Cell Research Center Microscopy core and Flow Cytometry Core, the Electron Microscopy Services Center of the UCLA Brain Research Institute (under the supervision of Sirus Kohan), and the statistical analyses were supported by the NIH National Center for Advancing Translational Sciences (NCATS) UCLA CTSI (UL1TR000124). Research reported in this publication includes work performed in the Jonsson Comprehensive Cancer Center Flow Cytometry Core facility supported by the National Cancer Institute (NCI) (P30CA016042).

Received: October 15, 2013
Revised: February 28, 2014
Accepted: May 20, 2014
Published: June 19, 2014

REFERENCES

Barreiro, E., Peinado, V.I., Galdiz, J.B., Ferrer, E., Marin-Corral, J., Sánchez, F., Gea, J., and Barberà, J.A.; ENIGMA in COPD Project (2010). Cigarette smoke-induced oxidative stress: A role in chronic obstructive pulmonary disease skeletal muscle dysfunction. Am. J. Respir. Crit. Care Med. *182*, 477–488.

Blanpain, C., Lowry, W.E., Pasolli, H.A., and Fuchs, E. (2006). Canonical notch signaling functions as a commitment switch in the epidermal lineage. Genes Dev. *20*, 3022–3035.

Borthwick, D.W., Shahbazian, M., Krantz, Q.T., Dorin, J.R., and Randell, S.H. (2001). Evidence for stem-cell niches in the tracheal epithelium. Am. J. Respir. Cell Mol. Biol. *24*, 662–670.

Cancer Genome Atlas Research Network (2012). Comprehensive genomic characterization of squamous cell lung cancers. Nature *489*, 519–525.

Chuikov, S., Levi, B.P., Smith, M.L., and Morrison, S.J. (2010). Prdm16 promotes stem cell maintenance in multiple tissues, partly by regulating oxidative stress. Nat. Cell Biol. *12*, 999–1006.

DeNicola, G.M., Karreth, F.A., Humpton, T.J., Gopinathan, A., Wei, C., Frese, K., Mangal, D., Yu, K.H., Yeo, C.J., Calhoun, E.S., et al. (2011). Oncogene-induced Nrf2 transcription promotes ROS detoxification and tumorigenesis. Nature *475*, 106–109.

Gao, X., Vockley, C.M., Pauli, F., Newberry, K.M., Xue, Y., Randell, S.H., Reddy, T.E., and Hogan, B.L. (2013). Evidence for multiple roles for grainyheadlike 2 in the establishment and maintenance of human mucociliary airway epithelium. Proc. Natl. Acad. Sci. USA *110*, 9356–9361.

Ghosh, M., Ahmad, S., Jian, A., Li, B., Smith, R.W., Helm, K.M., Seibold, M.A., Groshong, S.D., White, C.W., and Reynolds, S.D. (2013). Human tracheobronchial basal cells. Normal versus remodeling/repairing phenotypes in vivo and in vitro. Am. J. Respir. Cell Mol. Biol. *49*, 1127–1134.

Guseh, J.S., Bores, S.A., Stanger, B.Z., Zhou, Q., Anderson, W.J., Melton, D.A., and Rajagopal, J. (2009). Notch signaling promotes airway mucous metaplasia and inhibits alveolar development. Development *136*, 1751–1759.

He, S., Nakada, D., and Morrison, S.J. (2009). Mechanisms of stem cell self-renewal. Annu. Rev. Cell Dev. Biol. *25*, 377–406.

Hegab, A.E., Ha, V.L., Gilbert, J.L., Zhang, K.X., Malkoski, S.P., Chon, A.T., Darmawan, D.O., Bisht, B., Ooi, A.T., Pellegrini, M., et al. (2011). Novel stem/progenitor cell population from murine tracheal submucosal gland ducts with multipotent regenerative potential. Stem Cells *29*, 1283–1293.

Hegab, A.E., Ha, V.L., Attiga, Y.S., Nickerson, D.W., and Gomperts, B.N. (2012a). Isolation of basal cells and submucosal gland duct cells from mouse trachea. J. Vis. Exp. *Sep 14*, e3731.

Hegab, A.E., Ha, V.L., Darmawan, D.O., Gilbert, J.L., Ooi, A.T., Attiga, Y.S., Bisht, B., Nickerson, D.W., and Gomperts, B.N. (2012b). Isolation and in vitro characterization of basal and submucosal gland duct stem/progenitor cells from human proximal airways. Stem Cells Transl. Med. *1*, 719–724.

Herbst, R.S., Heymach, J.V., and Lippman, S.M. (2008). Lung cancer. N. Engl. J. Med. *359*, 1367–1380.

Hicks, C., Johnston, S.H., diSibio, G., Collazo, A., Vogt, T.F., and Weinmaster, G. (2000). Fringe differentially modulates Jagged1 and Delta1 signalling through Notch1 and Notch2. Nat. Cell Biol. *2*, 515–520.

Hochmuth, C.E., Biteau, B., Bohmann, D., and Jasper, H. (2011). Redox regulation by Keap1 and Nrf2 controls intestinal stem cell proliferation in Drosophila. Cell Stem Cell *8*, 188–199.

Hong, K.U., Reynolds, S.D., Watkins, S., Fuchs, E., and Stripp, B.R. (2004). Basal cells are a multipotent progenitor capable of renewing the bronchial epithelium. Am. J. Pathol. *164*, 577–588.

Jang, Y.Y., and Sharkis, S.J. (2007). A low level of reactive oxygen species selects for primitive hematopoietic stem cells that may reside in the low-oxygenic niche. Blood *110*, 3056–3063.

Kansanen, E., Kuosmanen, S.M., Leinonen, H., and Levonen, A.L. (2013). The Keap1-Nrf2 pathway: Mechanisms of activation and dysregulation in cancer. Redox Biol. *1*, 45–49.

Kim, J.H., Thimmulappa, R.K., Kumar, V., Cui, W., Kumar, S., Kombairaju, P., Zhang, H., Margolick, J., Matsui, W., Macvittie, T., et al. (2014). NRF2-mediated Notch pathway activation enhances hematopoietic reconstitution following myelosuppressive radiation. J. Clin. Invest. *124*, 730–741.

Le Belle, J.E., Orozco, N.M., Paucar, A.A., Saxe, J.P., Mottahedeh, J., Pyle, A.D., Wu, H., and Kornblum, H.I. (2011). Proliferative neural stem cells have high endogenous ROS levels that regulate self-renewal and neurogenesis in a PI3K/Akt-dependant manner. Cell Stem Cell *8*, 59–71.

Lee, J.M., Li, J., Johnson, D.A., Stein, T.D., Kraft, A.D., Calkins, M.J., Jakel, R.J., and Johnson, J.A. (2005). Nrf2, a multi-organ protector? FASEB J. *19*, 1061–1066.

Luxenburg, C., Pasolli, H.A., Williams, S.E., and Fuchs, E. (2011). Developmental roles for Srf, cortical cytoskeleton and cell shape in epidermal spindle orientation. Nat. Cell Biol. *13*, 203–214.

Malhotra, D., Thimmulappa, R., Navas-Acien, A., Sandford, A., Elliott, M., Singh, A., Chen, L., Zhuang, X., Hogg, J., Pare, P., et al. (2008). Decline in NRF2-regulated antioxidants in chronic obstructive pulmonary disease lungs due to loss of its positive regulator, DJ-1. Am. J. Respir. Crit. Care Med. *178*, 592–604.

Malkoski, S.P., Cleaver, T.G., Lu, S.L., Lighthall, J.G., and Wang, X.J. (2010). Keratin promoter based gene manipulation in the murine conducting airway. Int. J. Biol. Sci. *6*, 68–79.

McDonald, J.T., Kim, K., Norris, A.J., Vlashi, E., Phillips, T.M., Lagadec, C., Della Donna, L., Ratikan, J., Szelag, H., Hlatky, L., and McBride, W.H. (2010). Ionizing radiation activates the Nrf2 antioxidant response. Cancer Res. *70*, 8886–8895.

Morimoto, H., Iwata, K., Ogonuki, N., Inoue, K., Atsuo, O., Kanatsu-Shinohara, M., Morimoto, T., Yabe-Nishimura, C., and Shinohara, T. (2013). ROS are required for mouse spermatogonial stem cell self-renewal. Cell Stem Cell *12*, 774–786.

Myant, K.B., Cammareri, P., McGhee, E.J., Ridgway, R.A., Huels, D.J., Cordero, J.B., Schwitalla, S., Kalna, G., Ogg, E.L., Athineos, D., et al. (2013). ROS production and NF-κB activation triggered by RAC1 facilitate WNT-driven intestinal stem cell proliferation and colorectal cancer initiation. Cell Stem Cell *12*, 761–773.

Naka, K., Muraguchi, T., Hoshii, T., and Hirao, A. (2008). Regulation of reactive oxygen species and genomic stability in hematopoietic stem cells. Antioxid. Redox Signal. *10*, 1883–1894.

Nakamura, S., Oshima, M., Yuan, J., Saraya, A., Miyagi, S., Konuma, T., Yamazaki, S., Osawa, M., Nakauchi, H., Koseki, H., and Iwama, A. (2012). Bmi1 confers resistance to oxidative stress on hematopoietic stem cells. PLoS ONE *7*, e36209.

Nguyen, T., Nioi, P., and Pickett, C.B. (2009). The Nrf2-antioxidant response element signaling pathway and its activation by oxidative stress. J. Biol. Chem. *284*, 13291–13295.

Okawa, H., Motohashi, H., Kobayashi, A., Aburatani, H., Kensler, T.W., and Yamamoto, M. (2006). Hepatocyte-specific deletion of the keap1 gene activates Nrf2 and confers potent resistance against acute drug toxicity. Biochem. Biophys. Res. Commun. *339*, 79–88.

Ooi, A., Dykema, K., Ansari, A., Petillo, D., Snider, J., Kahnoski, R., Anema, J., Craig, D., Carpten, J., Teh, B.T., and Furge, K.A. (2013). CUL3 and NRF2 mutations confer an NRF2 activation phenotype in a sporadic form of papillary renal cell carcinoma. Cancer Res. *73*, 2044–2051.

Raj, L., Ide, T., Gurkar, A.U., Foley, M., Schenone, M., Li, X., Tolliday, N.J., Golub, T.R., Carr, S.A., Shamji, A.F., et al. (2011). Selective killing of cancer cells by a small molecule targeting the stress response to ROS. Nature *475*, 231–234.

Rock, J.R., and Hogan, B.L. (2011). Epithelial progenitor cells in lung development, maintenance, repair, and disease. Annu. Rev. Cell Dev. Biol. *27*, 493–512.

Rock, J.R., Onaitis, M.W., Rawlins, E.L., Lu, Y., Clark, C.P., Xue, Y., Randell, S.H., and Hogan, B.L. (2009). Basal cells as stem cells of the mouse trachea and human airway epithelium. Proc. Natl. Acad. Sci. USA *106*, 12771–12775.

Rock, J.R., Randell, S.H., and Hogan, B.L. (2010). Airway basal stem cells: a perspective on their roles in epithelial homeostasis and remodeling. Dis. Model. Mech. *3*, 545–556.

Rock, J.R., Gao, X., Xue, Y., Randell, S.H., Kong, Y.Y., and Hogan, B.L. (2011). Notch-dependent differentiation of adult airway basal stem cells. Cell Stem Cell *8*, 639–648.

Sakaue-Sawano, A., Kurokawa, H., Morimura, T., Hanyu, A., Hama, H., Osawa, H., Kashiwagi, S., Fukami, K., Miyata, T., Miyoshi, H., et al. (2008). Visualizing spatiotemporal dynamics of multicellular cell-cycle progression. Cell *132*, 487–498.

Satoh, H., Moriguchi, T., Taguchi, K., Takai, J., Maher, J.M., Suzuki, T., Winnard, P.T., Jr., Raman, V., Ebina, M., Nukiwa, T., and Yamamoto, M. (2010). Nrf2-deficiency creates a responsive microenvironment for metastasis to the lung. Carcinogenesis *31*, 1833–1843.

Snyder, J.C., Teisanu, R.M., and Stripp, B.R. (2009). Endogenous lung stem cells and contribution to disease. J. Pathol. *217*, 254–264.

Sporn, M.B., and Liby, K.T. (2012). NRF2 and cancer: the good, the bad and the importance of context. Nat. Rev. Cancer *12*, 564–571.

Suzuki, T., Motohashi, H., and Yamamoto, M. (2013). Toward clinical application of the Keap1-Nrf2 pathway. Trends Pharmacol. Sci. *34*, 340–346.

Thimmulappa, R.K., Mai, K.H., Srisuma, S., Kensler, T.W., Yamamoto, M., and Biswal, S. (2002). Identification of Nrf2-regulated genes induced by the chemopreventive agent sulforaphane by oligonucleotide microarray. Cancer Res. *62*, 5196–5203.

Tilley, A.E., Harvey, B.G., Heguy, A., Hackett, N.R., Wang, R., O'Connor, T.P., and Crystal, R.G. (2009). Down-regulation of the notch pathway in human airway epithelium in association with smoking and chronic obstructive pulmonary disease. Am. J. Respir. Crit. Care Med. *179*, 457–466.

Tsao, P.N., Vasconcelos, M., Izvolsky, K.I., Qian, J., Lu, J., and Cardoso, W.V. (2009). Notch signaling controls the balance of ciliated and secretory cell fates in developing airways. Development *136*, 2297–2307.

Wakabayashi, N., Shin, S., Slocum, S.L., Agoston, E.S., Wakabayashi, J., Kwak, M.K., Misra, V., Biswal, S., Yamamoto, M., and Kensler, T.W. (2010). Regulation of notch1 signaling by nrf2: implications for tissue regeneration. Sci. Signal. *3*, ra52.

Wang, K., Zhang, T., Dong, Q., Nice, E.C., Huang, C., and Wei, Y. (2013). Redox homeostasis: the linchpin in stem cell self-renewal and differentiation. Cell Death Dis. *4*, e537.

Westhoff, B., Colaluca, I.N., D'Ario, G., Donzelli, M., Tosoni, D., Volorio, S., Pelosi, G., Spaggiari, L., Mazzarol, G., Viale, G., et al. (2009). Alterations of the Notch pathway in lung cancer. Proc. Natl. Acad. Sci. USA *106*, 22293–22298.